









A Radiatively Quiet Glitch and Anti-glitch in the Magnetar 1E 2259+586

George Younes^{1,2} , Paul S. Ray³ , Matthew G. Baring⁴, Chryssa Kouveliotou^{1,2} , Corinne Fletcher⁵, Zorawar Wadiasingh⁶ ,
Alice K. Harding⁶ , and Adam Goldstein⁵ 

¹ Department of Physics, The George Washington University, Washington, DC 20052, USA; gyounes@gwu.edu

² Astronomy, Physics and Statistics Institute of Sciences (APSYS), The George Washington University, Washington, DC 20052, USA

³ Space Science Division, U.S. Naval Research Laboratory, Washington, DC 20375, USA

⁴ Department of Physics and Astronomy, Rice University, MS-108, P.O. Box 1892, Houston, TX 77251, USA

⁵ Science and Technology Institute, Universities Space Research Association, Huntsville, AL 35805, USA

⁶ Astrophysics Science Division, NASA Goddard Space Flight Center, Greenbelt, MD 20771, USA

Received 2020 March 26; revised 2020 June 5; accepted 2020 June 6; published 2020 June 22

Abstract

We report on the timing and spectral properties of the soft X-ray emission from the magnetar 1E 2259+586 from 2013 January, ~ 8 months after the detection of an anti-glitch, until 2019 September, using the Neil Gehrels Swift and Neutron star Interior Composition Explorer (NICER) observatories. During this time span, we detect two timing discontinuities. The first, occurring around 5 yr after the 2012 April anti-glitch, is a relatively large spin-up glitch with a fractional amplitude $\Delta\nu/\nu = 1.24(2) \times 10^{-6}$. We find no evidence for flux enhancement or change in the spectral or pulse-profile shape around the time of this glitch. This is consistent with the picture that a significant number of magnetar spin-up glitches are radiatively quiet. Approximately 1.5 yr later in 2019 April, 1E 2259+586 exhibited an anti-glitch with spin-down of a fractional amplitude $\Delta\nu/\nu = -5.8(1) \times 10^{-7}$, similar to the fractional change detected in 2012. We do not, however, detect any change to the pulse-profile shape or increase in the rms pulsed flux of the source, nor do we see any possible bursts from its direction around the time of the anti-glitch, all of which occurred during the 2012 event. Hence, similar to spin-up glitches, anti-glitches can occur silently. This may suggest that these phenomena originate in the neutron star interior, and that their locale and triggering mechanism do not necessarily have to be connected to the magnetosphere. Last, our observations suggest that the occurrence rate of spin-up and spin-down glitches is about the same in 1E 2259+586, with the former having a larger net fractional change.

Unified Astronomy Thesaurus concepts: [Magnetars \(992\)](#); [Neutron stars \(1108\)](#); [Compact objects \(288\)](#)

1. Introduction

Magnetars represent a subset of the isolated neutron star (ISN) family with a unique set of observational properties. Most show long spin periods ($P \sim 2\text{--}12$ s) and large spin-down rates ($\dot{P} \sim 10^{-13}\text{--}10^{-10}$ s s⁻¹), implying large surface dipole magnetic field strengths of the order of $\sim 10^{14}$ G, and young spin-down ages with an average of a few thousand years. Magnetars are usually observed as hot thermal X-ray emitters with surface blackbody temperatures of $kT \sim 0.5$ keV, and as bright persistent X-ray sources with $L_X \sim 10^{33}\text{--}10^{36}$ erg s⁻¹, exceeding their corresponding rotational energy losses ($|\dot{E}| \propto \dot{P}/P^3$). Hence, unlike their less-magnetic cousins, rotation-powered pulsars (RPPs), magnetars are believed to be powered through the decay of their large inferred surface and internal magnetic fields (see, e.g., Mereghetti et al. 2015; Turolla et al. 2015; Kaspi & Beloborodov 2017 for reviews).

A defining trait of the magnetar class is their recurring variability observed on broad timescales. They randomly enter burst-active episodes where they emit tens to hundreds of short (~ 0.2 s), bright ($L_{\text{peak}} \sim 10^{40}$ erg s⁻¹), hard X-ray bursts over the course of days to months. Coincident with these bursting episodes, an increase in their persistent X-ray emission by factors of few to a thousand is most often observed. At the same time, the persistent emission of magnetars undergoes changes to its spectral and temporal properties, which often recover exponentially back to quiescence over weeks to months timescales (e.g., Camero et al. 2014; Scholz et al. 2014; Younes et al. 2017b; Coti Zelati et al. 2018). We note that the above canonical characteristics are no longer restricted to typical (high dipolar B) magnetars and have

been recently observed from low- B magnetars (Rea et al. 2010), central compact objects (Borghese et al. 2018), and high- B RPPs (Archibald et al. 2016; Göğüş et al. 2016).

1E 2259+586 was discovered with the Einstein telescope in the supernova remnant (SNR) G109.1-1.0 (Fahlman & Gregory 1981). It has a spin period of $P \approx 7$ s and a spin-down rate of $\dot{P} = 4.8 \times 10^{-13}$ s s⁻¹, implying a surface polar field of $B \sim 1.2 \times 10^{14}$ G and a spin-down age of $P/(2\dot{P}) \sim 230$ kyr. In 2002, 1E 2259+586 entered a burst-active episode during which RXTE detected ~ 80 magnetar-like bursts (Kaspi et al. 2003). This discovery sealed the earlier results by Gavriil et al. (2002) on the unification of two classes of isolated neutron stars (INSSs), the soft gamma repeaters (SGRs), and the anomalous X-ray pulsars (AXPs), under the magnetar umbrella. The source has been regularly monitored in the soft X-ray band, first with RXTE, followed by with Swift. Apart from the outburst, 1E 2259+586 has shown a relatively high level of spectral and timing stability since its monitoring started in 1996, the latter interrupted by discontinuities at a rate of about 1 every 6 yr (Dib & Kaspi 2014).

In 2012, 1E 2259+586 entered an active episode where it showed both bursting activity as well as an increase in its X-ray flux accompanied by hardening of the spectrum (Archibald et al. 2013). During this episode, the source exhibited two discontinuities in its timing behavior. The first, occurring at outburst onset, can only be interpreted as an abrupt spin-down or anti-glitch event: a sudden decrease in spin frequency with a fractional change of $\Delta\nu/\nu \sim -3 \times 10^{-7}$. The second could either be due to a regular spin-up glitch or another spin-down event, depending on the timing model (see also Hu et al. 2014). Spin-down glitches are

exceptionally rare and have so far never been reported from any RPP, which have collectively shown hundreds of spin-up glitches (e.g., Espinoza et al. 2011).⁷ Apart from the 2012 event, another candidate spin-down glitch from 1E 2259+586 occurred in 2009 (Ícđem et al. 2011; Dib & Kaspi 2014), which was also accompanied by an elevated flux level from the source. Note also that an anti-glitch was reported from the magnetar 1E 1841–045 in archival RXTE data (Şaşmaz Muş et al. 2014); however, analysis by a different team of the same data set returned a null result (Dib & Kaspi 2014).

In this Letter, we report on our timing and spectral analyses of over 6.5 yr of Swift and 9 months of NICER data of the magnetar 1E 2259+586. During this span, the source has shown a relatively large spin-up glitch and an anti-glitch with a similar fractional change to the one detected in 2012. Both events are, however, radiatively quiet, contrasting the 2012 anti-glitch. The observations and data reduction are presented in Section 2. We summarize our results in Section 3, and in Section 4, we discuss the implications of our discovery, focusing on the anti-glitch triggering locale, i.e., internal versus external to the neutron star.

2. Observations and Data Reduction

1E 2259+586 was observed with NICER on a bi-weekly basis starting on 2019 March 17, as part of our magnetar monitoring program. NICER is a non-imaging X-ray timing instrument, sensitive to photons in the energy range 0.2–12 keV (Gendreau et al. 2016). It consists of 56 coaligned X-ray concentrating optics, covering a 30 arcmin² field of view, providing a collecting area of 1900 cm² at 1.5 keV (LaMarr et al. 2016). We processed NICER data using NICERDAS version 6, as part of HEASOFT version 6.26. For each observation, we created good time intervals from level 1 event files using standard filtering criteria, for example, requiring the source to be at least 30° from the Earth’s limb, and removing intervals around entry into and exit from the South Atlantic Anomaly (SAA). In all of our NICER analyses, we only include photons in the range of 0.8–8 keV. Due to the nonnegligible hydrogen column density toward 1E 2259+586 and its soft X-ray spectrum, the background emission dominates below ~0.8 keV and above ~8 keV, respectively. Finally, we removed MPU1 data from observation 2598041001 due to a time stamp anomaly, which occurred on 2019 July 16 during NICER passage through SAA. This anomaly did not affect any of our subsequent observations.

The Swift/X-ray Telescope (XRT) is a focusing CCD, sensitive to photons in the energy range of 0.2–10 keV (Burrows et al. 2005). All XRT observations we consider in this Letter were taken in windowed timing (WT) mode, which results in a 1D image with a time resolution of 1.7 ms (Evans et al. 2007). We reduced the data using XRTDAS version 3.5.0. We extracted source events from each good time interval (GTI) of a given observation separately, using a circular region with a 20 pixel radius centered on the brightest pixel of each 1D image. We extract background events from an annulus centered at the same position as the source with inner and outer radii of 80 and 120 pixels. For the spectral analysis we generated the ancillary files using xrtmkarf, and used the response matrices in CALDB v014. We excluded any GTI for which

the source landed within a 3 pixel distance from a bad column or the edge of the CCD. The remaining spectra for each observation were added together, along with the ancillary, background, and response files using the HEASOFT tool `addspec`.

We only perform spectral analysis on the Swift data. We use XSPEC version 12.10.1f (Arnaud 1996). To account for absorption toward the source, we use the Tübingen-Boulder interstellar medium absorption model (`tbabs`) along with the abundances of Wilms et al. (2000) and the photoelectric cross-sections of Verner et al. (1996). We group the spectra to have at least one count per spectral bin and use the Cash statistic (C-stat) in XSPEC for model parameter estimation and error calculation. We note that the background around 1E 2259+586 is dominated by the emission from the SNR G109.1–1.0 (CTB 109, considered the progenitor to 1E 2259+586), which increases in intensity with increasing distance away from the magnetar (and peaks around 3′ from the source location; e.g., Sasaki et al. 2004). Accordingly, our XRT background estimate, which incorporates part of the SNR up to 2′ away from the source, should be considered a conservative correction to the SNR contribution to the source flux. Nevertheless, this background is only a few percent of the source flux within our XRT source extraction region, even when considering the 0.8–2 keV energy range (e.g., Patel et al. 2001; Sasaki et al. 2004).

We refrain from performing spectral analysis with NICER given that it is not an imaging instrument: the background within the 30 arcmin² field of view requires detailed, nontrivial modeling. Along with the sky background, there is an unknown contribution from the supernova remnant that depends on the placement of the source within the field of view. Instead, for NICER observations, we rely on pulsed flux analysis to check for any variability in the source brightness level.

In total, we analyzed 117 Swift/XRT observations and 30 NICER observations covering the time range between 2013 January 20 and 2019 September 10. We quote the uncertainties of all spectral and timing model parameters at the 68% confidence level, unless otherwise noted.

3. Results

3.1. Timing

We relied on a prior Swift magnetar monitoring program (e.g., Archibald et al. 2013) to build a phase-coherent timing solution for the source. We analyze here all WT mode Swift/XRT observations of 1E 2259+586 since 2013 January 20 (observation ID 00032035053), the first observation after the last one reported in Archibald et al. (2013). We selected photons in the energy range 0.8–8 keV (for consistency with NICER; note that extending the energy range to 10 keV does not have any impact on our timing models), and corrected their arrival times to the solar barycenter using the source best sky location (Hulleman et al. 2001). We then performed our phase-coherent timing analysis following a phase-fitting technique (e.g., Dall’Osso et al. 2003). The source pulse phase evolution is described by

$$\phi(t) = \phi_0 + \nu(t - t_0) + \frac{1}{2}\dot{\nu}(t - t_0)^2 + \frac{1}{6}\ddot{\nu}(t - t_0)^3 + \dots, \quad (1)$$

truncated to the highest statistically significant term. We first establish a spin period with a high level of accuracy utilizing

⁷ <http://www.jb.man.ac.uk/pulsar/glitches/gTable.html>; <https://www.atnf.csiro.au/research/pulsar/psrcat/glitchTbl.html>

Table 1
Phase-coherent Spin Parameters of 1E 2259+586

MJD Range	56312–57947	57968–58574
Epoch (MJD)	57934.48	58359.56
ν (Hz)	0.143 282 728 7(3)	0.143 282 545 6(2)
$\dot{\nu}$ (Hz s ⁻¹)	$-9.84(5) \times 10^{-15}$	$-9.75(2) \times 10^{-15}$
$\ddot{\nu}$ (Hz s ⁻²)	$-1.8(3) \times 10^{-23}$	$1.4(3) \times 10^{-23}$
$d^3\nu/dt^3$ (Hz s ⁻³)	$-6(1) \times 10^{-31}$...
$d^4\nu/dt^4$ (Hz s ⁻⁴)	$-6(1) \times 10^{-39}$...
χ^2/dof	117/87	31/39
rms residual (cycle)	0.011	0.0072

Note. The MJD ranges are for inter-glitch epochs. The 1σ uncertainty on each parameter is given in parentheses.

several observations closely spaced in time. The phase drift in such a select case is fit to the linear term of Equation (1) and the spin frequency is corrected accordingly. As more observations are added, the error on the spin frequency decreases, until the phase drift is dominated by a spin-down term. A second term of Equation (1) is then added to the model and the procedure is continued.

Following the method above, we were able to successfully phase connect all Swift observations from 2013 January 20 (MJD 56,312) to 2017 July 13 (MJD 57,947), when our model failed to accurately predict the phase of the subsequent observations, indicating the occurrence of a sudden timing discontinuity. Our timing model spanning this date range required terms up to the fourth frequency derivative from Equation (1). We find a reduced chi-square, χ^2_ν , of 1.37 for 87 degrees of freedom (dof) and an unweighted rms of 0.011 cycles. The best-fit model parameters are summarized in Table 1, while the residuals are shown in the left panel of Figure 1. Excluding the last term from our model results in a slightly worse fit with a χ^2_ν of 1.51 for 88 dof and an rms of 0.013 cycles. We note that our timing model during this time span predicts a spin frequency for the last observation reported in Archibald et al. (2013) that is consistent at the 1σ and 3σ levels with their timing models 1 and 2, respectively.

To accurately describe the discontinuity that occurred after the 2017 July 13 observation, we focus our analysis on a time range centered on this date and extending 9 months before and after the anomaly.⁸ The upper left panel of Figure 2 shows the phase residuals for all observations after subtracting a model consisting of ν and $\dot{\nu}$ as measured within the 9 month observation prior to the first anomaly epoch. The subsequent drift in the pulse phase is linear in time indicating the presence of a glitch dominated by a sudden change in the spin frequency. We fit the full 18 month data set with a model consisting of ν , $\dot{\nu}$, and a glitch model of the form

$$\nu(t) = \nu_t + \Delta\nu + \Delta\dot{\nu}(t - t_g), \quad (2)$$

where $\Delta\nu$ and $\Delta\dot{\nu}$ are the resultant (semi-permanent) changes in spin frequency and its derivative, t_g is the glitch epoch, and ν_t is the predicted spin frequency prior to the glitch. We find a good fit to the phase drifts with a χ^2_ν of 1.09 for 34 dof, and an unweighted rms of 0.0092 cycles. The middle left panel of Figure 2 shows the

residuals in seconds of the best-fit model. We find the glitch epoch $t_g = 57967.2(8)$ MJD, i.e., 2017 August 2. We find a change in spin frequency $\Delta\nu = 1.78(2) \times 10^{-7}$ Hz s⁻¹, and in spin-down $\Delta\dot{\nu} = -3(2) \times 10^{-16}$ Hz s⁻². We caution that this latter component is required by the data only at the 2σ level according to an F-test and may not represent a true change in $\dot{\nu}$ but may simply account for some timing noise present when considering long stretches of the data. We note that the ν and $\dot{\nu}$ we derive during this time span are consistent within 2σ with the values derived in the first inter-glitch timing model (Table 1, second column).

We built a phase-coherent timing model for the data starting with the first observation after the glitch epoch, 2017 August 3 (57968 MJD), and up to 2019 April 1 (58574 MJD). The phase drift in this time span is well fit with a model consisting of three terms of Equation (1). We find a χ^2_ν of 0.81 for 39 dof with an rms of 0.0072 cycles. The timing solution that best describes the spin evolution of 1E 2259+586 during this time span is summarized in Table 1, while the residuals are shown in the right panel of Figure 1. However, this model does not successfully predict the pulse arrival times of the NICER observations after 2019 April 1, indicating the detection of another anomaly.

Similar to our above method, we focus our phase-coherent timing analysis around the time of the discontinuity. We include data spanning 10 months prior to the 2019 April 1 observation, and up to the 2019 September 10 NICER observation (a total baseline of 16 months). A model consisting of a ν and $\dot{\nu}$ describes well the phase evolution of the source up to the time of discontinuity. The phase shifts according to this model are shown in the upper right panel of Figure 2, where it is clear that the true pulse arrival time of subsequent observations is lagging behind the predicted one. Moreover, the phase shifts in all the following NICER observations evolve linearly with time, implying a sudden, in this case negative, jump in the spin frequency, i.e., the presence of an anti-glitch.

We fit the full 16 month data set with a model consisting of ν , $\dot{\nu}$, and a sudden change in ν , i.e., the first term of Equation (2). We find a good fit to the data with a χ^2_ν of 1.27 for 26 dof and an rms of 0.0065 cycles. The best-fit sudden frequency change is $\Delta\nu = -8.3(1) \times 10^{-8}$ Hz s⁻¹, with a fractional change $\Delta\nu/\nu = -5.8 \times 10^{-7}$. Given the good observational coverage around the anti-glitch, we constrain its epoch to within half a day, at 58574.5(5) MJD, i.e., 2019 April 1. The best-fit parameters of the full model are summarized in Table 2, while the residuals in seconds are shown in the middle right panel of Figure 2. Including a sudden change in the frequency derivative at the time of the anti-glitch does not improve the quality of the fit. Moreover, the ν and $\dot{\nu}$ derived through this model are consistent within 1σ with the ones derived in our second inter-glitch epoch (Table 1, rightmost column). Finally, we note that we do not detect any changes to the pulse-profile shape in the observations following either the spin-up or the spin-down glitch, nor do we find any energy-dependent variability; hence, there is no confusion in the timing model due to pulse counting.

3.2. Spectroscopy

To check for variability around the 2017 August spin-up glitch epoch, we relied on the spectra of all prior Swift/XRT

⁸ This baseline should suffice to properly constrain the anomaly parameters, search for any strong timing noise around this time, and constrain the presence of any exponentially recovering frequency change.

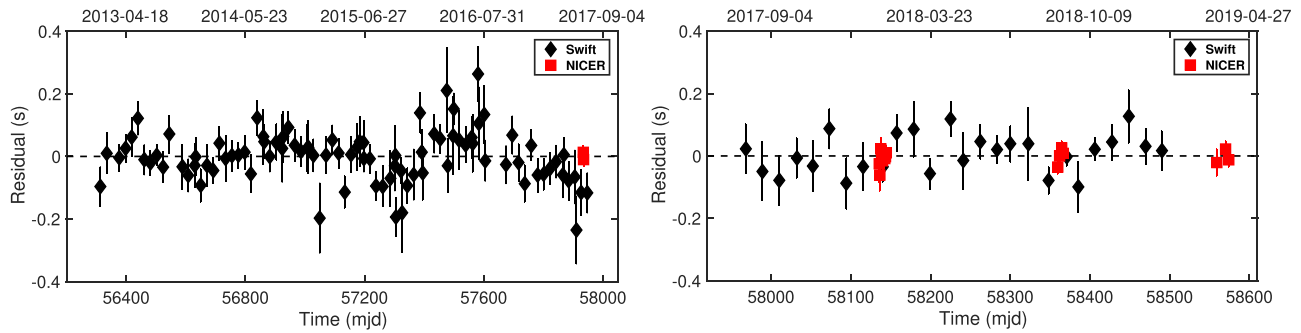


Figure 1. Timing residuals for the two epochs in Table 1. Left panel: dates are from 2013 January to 2017 July. The best-fit model includes contributions from the first five terms of Equation (1). Right panel: dates are from 2017 August to 2019 April. Three frequency terms are included in the best-fit model. See Table 1 for more details.

observations that were employed to measure the glitch parameters (Figure 2, left panels). We simultaneously fit the 0.8–10 keV spectra with an absorbed blackbody (BB) plus power-law (PL) model. We link the hydrogen column density between all observations and find $N_{\text{H}} = (0.91 \pm 0.03) \times 10^{22} \text{ cm}^{-2}$. The BB temperature kT ranged between 0.40 and 0.44 keV with an average 1σ uncertainty of about 0.02, while we find a photon index Γ between 2.6 and 3.4 and an average 1σ uncertainty of 0.5. These values are typical of 1E 2259+586 as inferred with, e.g., XMM-Newton (Pizzocaro et al. 2019). The 2–10 keV absorption-corrected fluxes of these spectra are shown in the lower left panel of Figure 2. The dashed horizontal line is the average value and corresponds to $F_{\text{avg}} = (1.7 \pm 0.1) \times 10^{-11} \text{ erg cm}^{-2} \text{ s}^{-1}$. We fit the subsequent Swift/XRT observations simultaneously with the same model, while fixing the hydrogen column density to the value as derived from the pre-glitch fit.⁹ The absorption-corrected 2–10 keV flux of these spectra are also shown in the lower left panel of Figure 2. It is clear that these fluxes follow the pre-glitch average flux well, implying that no flux variability occurred at or shortly after the glitch epoch. The temperature of the BB component and the PL indices were also within the uncertainties of the values derived in the pre-glitch data. For completeness, we also verified that the rms pulsed flux does not show any variability around the glitch epoch.

We relied on the rms pulsed flux (e.g., Dib & Kaspi 2014; Section 2) to search for any spectral changes around the anti-glitch. The lower right panel of Figure 2 shows the 0.8–8 keV rms pulsed flux (not background corrected) of all NICER - observations that were used to characterize the anti-glitch timing parameters. We also measured the 0.8–10 keV rms pulsed flux of all Swift/XRT observations, and multiplied the results by a constant normalization of $F_{\text{rms,n}}/F_{\text{rms,s}} \approx 16$, where $F_{\text{rms,n}}$ and $F_{\text{rms,s}}$ are the pre-glitch average of the NICER rms pulsed fluxes and the average of the Swift/XRT rms pulsed fluxes, respectively. The NICER post-glitch rms pulsed fluxes follow well the expected average as measured with the pre-glitch data (dashed line in Figure 2, lower right panel) implying the absence of pulsed flux variability at or following the time of the anti-glitch. We note that the Swift spectra during this time span are consistent with the ones measured around the glitch epoch, and with the long-term quiescent spectral properties of the source.

⁹ Fixing N_{H} better constrains small flux variations that may be masked by allowing the column density to vary. We verified that allowing N_{H} to vary does not change any of our results.

3.3. Burst Search

We utilized Fermi-Gamma-ray Burst Monitor (GBM) to search for magnetar-like bursts ± 5 days around the dates of the two discontinuities, using the CTIME data type (0.256 s temporal resolution) in an energy range 10–100 keV. Our search algorithm is based on Gavril et al. (2004), which calculates the Poisson probability for an event to be a random fluctuation around a background-corrected mean, flagging any low probability events as possible bursts. Throughout the 20 day period, we find 29 candidate bursts. In order to determine if these events were related to 1E 2259+586, we used the Fermi-GBM subthreshold search, referred to as the Targeted Search (Goldstein et al. 2019), to follow up these times and provide sky localizations for those candidates. The Targeted Search utilizes continuous time-tagged event (CTTE) data with $2 \mu\text{s}$ precision to search ± 30 s around a given time.

We do not find any of the 29 burst candidates to be spatially coincident at the 90% level with the location of 1E 2259+586. The GBM lower limit for the detection of a magnetar-like burst in the energy range 10–100 keV is $\sim 1.0 \times 10^{-7} \text{ erg s}^{-1} \text{ cm}^{-2}$ (e.g., van der Horst et al. 2012), which would translate to a luminosity of about $2.0 \times 10^{38} \text{ erg s}^{-1}$ at the 3.2 kpc distance of 1E 2259+586 (Kotthes & Foster 2012). This is one order of magnitude smaller than the luminosity of the GBM burst detected from 1E 2259+586 at the 2012 anti-glitch epoch (Foley et al. 2012). Hence, we can exclude the possibility of a similar short burst around the time of this latest anti-glitch, as well as at the time of the 2017 glitch, unless it occurred during GBM Earth-occulted periods, which make up 20% of the time. Also, we cannot exclude the possibility of fainter short bursts akin to the ones detected from several magnetars with NuSTAR (e.g., An et al. 2014; Younes et al. 2020).

4. Summary and Discussion

In this Letter, we have analyzed over 6 yr of monitoring data of the magnetar 1E 2259+586 taken with Swift-XRT and NICER, starting from the Swift observation taken on 2013 January 20, and up to 2019 September 10. Following a relatively quiet period that lasted for about five years after the 2012 anti-glitch, the source showed in 2017 August a large glitch, dominated by a sudden spin-up jump in rotational frequency with a fractional change of the order of $1.24(2) \times 10^{-6}$ that exhibits no evidence of a “healing” recovery in its ephemeris. The glitch was not accompanied with any spectral or temporal changes, and we did not detect any magnetar-like bursts with Fermi-GBM from the

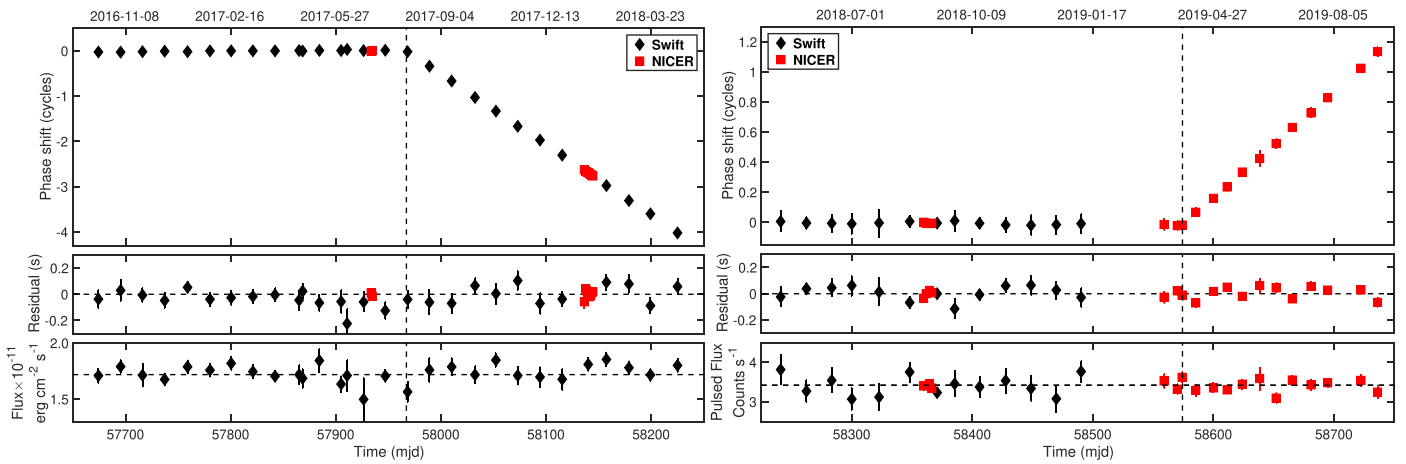


Figure 2. Upper left panel: timing residuals around the 2017 August glitch after subtracting a model consisting of ν and $\dot{\nu}$ that best fit the pre-glitch data. Middle left panel: timing residuals when including a glitch to the timing model (Table 2, second column). The rms of the best fit is 0.0089 cycles. Lower left panel: absorption-corrected 2–10 keV flux as derived using Swift/XRT. The horizontal line is the average flux as derived with pre-glitch data. The vertical dotted line in all three panels represents the glitch epoch. Upper right panel: timing residuals around the 2019 April glitch after subtracting a model consisting of ν and $\dot{\nu}$ that best fit the pre-glitch data. Middle right panel: timing residuals when including a glitch to the timing model (Table 2, third column). The rms of the best fit is 0.0065 cycles. Lower right panel: NICER 0.8–8 keV rms pulsed flux. The horizontal dashed line is the average pulsed flux for the NICER pre-glitch data. The Swift/XRT pulsed fluxes are normalized to this average. The vertical dotted line in all three panels represents the anti-glitch epoch. See the text for more details.

Table 2
Spin Parameters around Glitch Epochs

MJD range	57674–58225	58241–58736
Epoch (MJD)	57934.48	58359.56
ν (Hz)	0.143 282 729 9(9)	0.143 282 546 2(6)
$\dot{\nu}$ (Hz s ⁻¹)	$-9.6(1) \times 10^{-15}$	$-9.74(6) \times 10^{-15}$
t_g (MJD)	57967.2(8)	58574.5(5)
$\Delta\nu$ (Hz)	$1.78(2) \times 10^{-7}$	$-8.3(1) \times 10^{-8}$
$\Delta\dot{\nu}$ (Hz s ⁻¹)	$-3(2) \times 10^{-16}$...
$\Delta\nu/\nu$	$1.24(2) \times 10^{-6}$	$-5.8(1) \times 10^{-7}$
χ^2/dof	33/34	33/26
rms residual (cycle)	0.0089	0.0065

Note. The MJD ranges encompass glitch epochs. The 1σ uncertainty on each parameter is given in parentheses.

direction of the source in a 10-day interval around the glitch epoch down to a limiting flux of $\sim 1.0 \times 10^{-7} \text{ erg cm}^{-2} \text{ s}^{-1}$.

Although a nonnegligible fraction of magnetar glitches occurs during periods of outbursts (e.g., Archibald et al. 2017), many are observed in isolation, in the absence of any form of activity (Dib & Kaspi 2014). This is reminiscent of glitches observed from young RPPs, where all glitch events (barring those detected from the two high-B pulsars that showed magnetar-like activity, PSR J1846–20, Gavriil et al. 2008; and PSR J1119+6127, Weltevrede et al. 2011) occurred “silently,” without any measurable change to their emission (Lyne et al. 2000; Espinoza et al. 2011; Yu et al. 2013). Consequently, the origin of impulsive spin-up glitches is thought to be internal, involving a transfer of angular momentum and rotational kinetic energy from the fast-rotating inner superfluid to the outer crust; these near-surface layers slow down faster due to external magnetic dipole braking torques. This picture also offers a plausible scenario for spin-up glitches in magnetars. Yet it does not a priori account for radiative changes occurring in tandem with glitches. Such activity, when correlated with abrupt changes in the timing solution, likely signal a physical connection between the zones of angular momentum/energy

transfer and magnetic field lines that thread the crust through to the magnetosphere. Mobility of heat/energy transfer is enhanced along field lines in neutron stars, and thus a coupling of surface and magnetospheric (burst) activity to spin-up glitches suggests a concomitant threading of field lines deeper into the crust proximate to the superfluid zones.

The timing solution following the spin-up glitch was robust enough to predict the pulse arrival times up to 2019 April 1. The subsequent observations indicate that a sudden spin-down glitch occurred, with the pulse progressively lagging its predicted arrival time. The lag increased monotonically with time implying a spin-down glitch dominated by a change in rotational frequency. The fractional change of this most recent anti-glitch is $-5.8(1) \times 10^{-7}$, similar to the one detected in 2012 (Archibald et al. 2013; Hu et al. 2014). However, there are some notable differences between the two events. During the 2012 anti-glitch, 1E 2259+586 entered an active period; the 2–10 keV flux increased by a factor of 2, the spectrum exhibited hardening, the shape of the pulse profile changed, and typical short magnetar-like bursts were detected from the direction of the source with Fermi-GBM. On the other hand, we do not detect any of the above activity during the most recent anti-glitch. While short bursts could have occurred during GBM Earth-occulted periods or below its sensitivity level, our NICER observations should have been able to detect any changes to the pulsed flux, pulse-profile shape, and/or spectral properties of the source. This result shows that an anti-glitch, similar to spin-up glitches, can indeed occur in isolation, outside of outburst periods.

An interesting aspect of some of the magnetar and high-B pulsar spin-up glitches detected at the onset of outburst activity (e.g., PSR J1119+6127, Archibald et al. 2018; 4U 0142+61, Gavriil et al. 2011; Archibald et al. 2017) is their over-recovery following the glitch. Hence, the long-term effect on the rotational frequency is a net spin-down. Assuming that the 2012 anti-glitch was due to an over-recovery from a spin-up glitch, Archibald et al. (2013) placed a 4 day 3σ upper limit on the over-recovery timescale for a glitch size of 1.0×10^{-6} . Here, we place a slightly smaller 3σ upper limit of 3 days for

the recovery of a glitch with the same size, which again is much smaller than the typical weeks to months-long recovery usually observed for spin-up glitches.

Anti-glitches can be the result of interplay between differentially rotating portions of neutron stars, and/or adjustments to the oblateness and moments of inertia of different regions. Extant interpretations of anti-glitches center on two scenarios, although we note that there is also the competing solid-body impact model of Huang & Geng (2014). The first main paradigm is that adopted by Garcia & Ranea-Sandoval (2015) and Mastrano et al. (2015) to address the 1E 2259 + 586 event in 2012, where adjustments in toroidal fields deep in the crust driven by build up of magnetic tension lead to small but abrupt changes in the overall oblateness of the star. The “twisted torus” field components inflate the rotating star a little and yield metastable, slightly prolate configurations that over time reach a critical strain that cracks the crust. This irrepressible change reorganizes the internal field to generate a slightly more spherical configuration of lower net moment of inertia, yielding an impulsive frequency spin-up. The observed $|\Delta\nu/\nu| \sim 3 \times 10^{-7}$ suggested that the toroidal fields are of the order of $\gtrsim 10^{15}$ Gauss in strength (i.e., higher than the surface fields), and that the magnetic energy released exceeded the observed radiative signal by a factor of ~ 5 .

The second picture is along the lines of more traditional models for normal radio pulsar glitches in that the events are connected to vortex reconfiguration/unpinning in the interior neutron superfluid zone but close to the crust: see Thompson et al. (2000) for a presentation in the context of the giant flare from SGR 1900 + 14. Kantor & Gusakov (2014) discuss how the velocity difference between the superfluid and normal stellar components can impact the degenerate energy and mass density configuration. They observe that vortex unpinning can actually precipitate anti-glitches for some particular stellar differential rotation profiles, yielding a deceleration in the rotation of both the superfluid and crustal regions. The associated adjustment of the radial density profile and the moment of inertia of the superfluid is coupled to an increase in the number of Cooper pairs. Kantor & Gusakov (2014) find that anti-glitches are more likely if the differential rotation between core and crust is greater, and also if the superfluid core temperature is larger, nominally, $\gtrsim 5 \times 10^7$ K.

In both scenarios, the site of crustal cracking and dissipation will determine its connection to poloidal field lines and thereby develop a geometric dichotomy for whether or not there would be an associated energy release into the magnetosphere. In the case of the 2019 “orphan” anti-glitch event with no accompanying radiative enhancement, we suggest that the internal adjustment locale is likely remote from the magnetic poles, and the reconfiguration energy is deposited via heating of deep subsurface regions.

Yet, if the anti-glitch is accompanied by plasma ejection into the magnetosphere, any increase in particle flux along open field lines would raise torques on the star at the light cylinder (Harding et al. 1999), also contributing to a net spin-down. Since the rotationally powered contribution to the energetics of the magnetar is fractionally small, it is difficult to calibrate any particle flux changes possibly associated with an anti-glitch. Such enhanced winds could alter the flaring of the open field line regions, possibly inducing changes in both the hard X-ray persistent emission pulse profile and flux. Unfortunately, there were no NuSTAR observations made in an epoch straddling the anti-

glitch. Thus a hard X-ray observational diagnostic on changes in the magnetospheric wind properties is not afforded by this event.

Regardless of the origin and the physical mechanism triggering the anti-glitches, 1E 2259+586 must be unique in its internal structure. Our detection of the spin-up and spin-down glitches from 1E 2259+586 during the last 6 years of monitoring demonstrates that the source undergoes each timing discontinuity at a comparable rate, with the former having a larger net fractional change. Throughout the full monitoring campaign that was initiated with RXTE starting in 1997 (Kaspi et al. 2003), 1E 2259+586 has so far shown three spin-up glitches and at least two spin-down glitches, and three if we include the candidate 2009 event (we excluded the 2012 second timing discontinuity here given that it could be interpreted as either a glitch or anti-glitch). No other isolated neutron star has ever shown such a sudden spin-down event, barring the disputed detection in the magnetar 1E 1841–045 (Dib & Kaspi 2014; Şaşmaz Muş et al. 2014).

Compared to the rest of the magnetar population, 1E 2259 + 586 is an archetypal source. Its outburst activity is representative of the population; it underwent two typical magnetar outbursts in the last ~ 25 yr (Kaspi et al. 2003; Archibald et al. 2013). In quiescence, its broadband X-ray spectrum is well described by a quasi-thermal soft X-ray part and a hard X-ray tail, similar to almost all magnetars (e.g., Kuiper et al. 2006; Enoto et al. 2017; Younes et al. 2017a), while its timing properties are relatively stable, following the expected trend of lower timing noise with increasing spin-down age (e.g., Cerri-Serim et al. 2019). Hence, it is not clear what allows 1E 2259+586 to undergo anti-glitch events compared to other magnetars, and at such a high rate. One noteworthy source in this regard is the accreting ultraluminous X-ray source NGC 300 ULX1, which showed a number of anti-glitches during its most recent outburst (Ray et al. 2019). However, in that case the anti-glitches came in the context of a neutron star being spun up extremely rapidly, so an anti-glitch is the natural consequence of the superfluid interior lagging in that spin-up. This cannot be the mechanism at work for 1E 2259+586 given that it is spinning down relatively consistently. Continuing to monitor 1E 2259+586 and the other bright magnetars is critical to better understand the causes of these distinctive events.

We thank for the referee for comments helpful to the polishing of the manuscript. G.Y. acknowledges support from NASA under NICER Guest Observer cycle-1 program 2098, grant number 80NSSC19K1452. M.G.B. acknowledges the generous support of the NSF through grant AST-1813649. NICER work at NRL is supported by NASA.

ORCID iDs

George Younes  <https://orcid.org/0000-0002-7991-028X>

Paul S. Ray  <https://orcid.org/0000-0002-5297-5278>

Chryssa Kouveliotou  <https://orcid.org/0000-0003-1443-593X>

Zorawar Wadiasingh  <https://orcid.org/0000-0002-9249-0515>

Alice K. Harding  <https://orcid.org/0000-0001-6119-859X>

Adam Goldstein  <https://orcid.org/0000-0002-0587-7042>

References

- An, H., Kaspi, V. M., Beloborodov, A. M., et al. 2014, *ApJ*, 790, 60
 Archibald, R. F., Kaspi, V. M., Ng, C.-Y., et al. 2013, *Natur*, 497, 591
 Archibald, R. F., Kaspi, V. M., Scholz, P., et al. 2017, *ApJ*, 834, 163

- Archibald, R. F., Kaspi, V. M., Tendulkar, S. P., & Scholz, P. 2016, *ApJL*, **829**, L21
- Archibald, R. F., Kaspi, V. M., Tendulkar, S. P., & Scholz, P. 2018, *ApJ*, **869**, 180
- Arnaud, K. A. 1996, in ASP Conf. Ser. 101: Astronomical Data Analysis Software and Systems V, ed. G. H. Jacoby & J. Barnes (San Francisco, CA: ASP), 17
- Borghese, A., Coti Zelati, F., Esposito, P., et al. 2018, *MNRAS*, **478**, 741
- Burrows, D. N., Hill, J. E., Nousek, J. A., et al. 2005, *SSRv*, **120**, 165
- Camero, A., Pappitto, A., Rea, N., et al. 2014, *MNRAS*, **438**, 3291
- Ceri-Serim, D., Serim, M. M., Şahiner, Ş., Inam, S. Ç., & Baykal, A. 2019, *MNRAS*, **485**, 2
- Coti Zelati, F., Rea, N., Pons, J. A., Campana, S., & Esposito, P. 2018, *MNRAS*, **474**, 961
- Dall'Osso, S., Israel, G. L., Stella, L., Possenti, A., & Peruzzi, E. 2003, *ApJ*, **599**, 485
- Dib, R., & Kaspi, V. M. 2014, *ApJ*, **784**, 37
- Enoto, T., Shibata, S., Kitaguchi, T., et al. 2017, *ApJS*, **231**, 8
- Espinoza, C. M., Lyne, A. G., Stappers, B. W., & Kramer, M. 2011, *MNRAS*, **414**, 1679
- Evans, P. A., Beardmore, A. P., Page, K. L., et al. 2007, *A&A*, **469**, 379
- Fahlman, G. G., & Gregory, P. C. 1981, *Natur*, **293**, 202
- Foley, S., Kouveliotou, C., Kaneko, Y., & Collazzi, A. 2012, GCN, **13280**, 1
- Garcia, F., & Ranea-Sandoval, I. F. 2015, *MNRAS*, **449**, L73
- Gavriil, F. P., Dib, R., & Kaspi, V. M. 2011, *ApJ*, **736**, 138
- Gavriil, F. P., Gonzalez, M. E., Gotthelf, E. V., et al. 2008, *Sci*, **319**, 1802
- Gavriil, F. P., Kaspi, V. M., & Woods, P. M. 2002, *Natur*, **419**, 142
- Gavriil, F. P., Kaspi, V. M., & Woods, P. M. 2004, *ApJ*, **607**, 959
- Gendreau, K. C., Arzoumanian, Z., Adkins, P. W., et al. 2016, *Proc. SPIE*, **9905**, 99051H
- Goldstein, A., Hamburg, R., Wood, J., et al. 2019, arXiv:1903.12597
- Göğüş, E., Lin, L., Kaneko, Y., et al. 2016, *ApJL*, **829**, L25
- Harding, A. K., Contopoulos, I., & Kazanas, D. 1999, *ApJL*, **525**, L125
- Hu, Y.-M., Pitkin, M., Heng, I. S., & Hendry, M. A. 2014, *ApJL*, **784**, L41
- Huang, Y. F., & Geng, J. J. 2014, *ApJL*, **782**, L20
- Hulleman, F., Tennant, A. F., van Kerkwijk, M. H., et al. 2001, *ApJL*, **563**, L49
- İçdem, B., Inam, S., & Baykal, A. 2011, *MNRAS*, **415**, 1523
- Kantor, E. M., & Gusakov, M. E. 2014, *ApJL*, **797**, L4
- Kaspi, V. M., & Beloborodov, A. 2017, *ARA&A*, **55**, 261
- Kaspi, V. M., Gavriil, F. P., Woods, P. M., et al. 2003, *ApJL*, **588**, L93
- Kothes, R., & Foster, T. 2012, *ApJL*, **746**, L4
- Kuiper, L., Hermsen, W., den Hartog, P. R., & Collmar, W. 2006, *ApJ*, **645**, 556
- LaMarr, B., Prigozhin, G., Remillard, R., et al. 2016, *Proc. SPIE*, **9905**, 99054W
- Lyne, A. G., Shemar, S. L., & Smith, F. G. 2000, *MNRAS*, **315**, 534
- Mastrano, A., Suvorov, A. G., & Melatos, A. 2015, *MNRAS*, **453**, 522
- Mereghetti, S., Pons, J. A., & Melatos, A. 2015, *SSRv*, **191**, 315
- Patel, S. K., Kouveliotou, C., Woods, P. M., et al. 2001, *ApJL*, **563**, L45
- Pizzocaro, D., Tiengo, A., Mereghetti, S., et al. 2019, *A&A*, **626**, A39
- Ray, P. S., Guillot, S., Ho, W. C. G., et al. 2019, *ApJ*, **879**, 130
- Rea, N., Esposito, P., Turolla, R., et al. 2010, *Sci*, **330**, 944
- Sasaki, M., Plucinsky, P. P., Gaetz, T. J., et al. 2004, *ApJ*, **617**, 322
- Şaşmaz Muş, S., Aydın, B., & Göğüş, E. 2014, *MNRAS*, **440**, 2916
- Scholz, P., Kaspi, V. M., & Cumming, A. 2014, *ApJ*, **786**, 62
- Thompson, C., Duncan, R. C., Woods, P. M., et al. 2000, *ApJ*, **543**, 340
- Turolla, R., Zane, S., & Watts, A. L. 2015, *RPPh*, **78**, 116901
- van der Horst, A. J., Kouveliotou, C., Gorgone, N. M., et al. 2012, *ApJ*, **749**, 122
- Verner, D. A., Ferland, G. J., Korista, K. T., & Yakovlev, D. G. 1996, *ApJ*, **465**, 487
- Weltevrede, P., Johnston, S., & Espinoza, C. M. 2011, *MNRAS*, **411**, 1917
- Wilms, J., Allen, A., & McCray, R. 2000, *ApJ*, **542**, 914
- Younes, G., Baring, M. G., Kouveliotou, C., et al. 2017a, *ApJ*, **851**, 17
- Younes, G., Baring, M. G., Kouveliotou, C., et al. 2020, *ApJL*, **889**, L27
- Younes, G., Kouveliotou, C., Jaodand, A., et al. 2017b, *ApJ*, **847**, 85
- Yu, M., Manchester, R. N., Hobbs, G., et al. 2013, *MNRAS*, **429**, 688